Correlation between intrinsic peak luminosity and spectral peak energy for energetic *Fermi* GRBs

Feraol Fana Dirirsa[†,∗] **and Soebur Razzaque**

Department of Physics, University of Johannesburg, Auckland Park 2006, South Africa
E-mail: [†]fdirirsa@uj.ac.za

We select energetic GRBs detected by *Fermi*-LAT/GBM with known redshift and compute the correlation between the intrinsic peak luminosity ($L_{\rm iso}$) and peak energy ($E_{\rm i,p}$) of the νF_ν energy spectrum, known as the Yonetoku relation, in the 1 keV–10 MeV and 1 keV–30 MeV energy ranges. This correlation has the potential to make GRBs standard candles, similar to type Ia supernovae, but extending to high redshift. We explore parameters of the Lambda-Cold-Dark-Matter cosmological model at high redshift using Yonetoku relation for our sample of GRBs.

[∗]Speaker.

1. Introduction

One of the strong correlations among the spectral parameters of gamma-ray bursts (GRBs) exists between the spectral peak energy of the νF_ν prompt spectrum and the isotropic peak luminosity L_{iso}, the so-called Yonetoku relation [1]. This correlation is valid for long GRBs (i.e., bursts with observed duration $\gtrsim 2$ s). The possibility to use this correlation makes it very relevant to standardizing the GRB energetics, making them cosmological tools and understanding their burst physics. However, there is no consensus yet on the physical interpretation of this correlation. The possible presence of selection effects, lack of sufficient sample of GRBs with known redshift, limited energy range provided by previous telescopes are also the main issues against validation of this correlation and its use as a cosmological tool. But the small dispersion of long GRBs around the power-law best fit line is encouraging.

Since the launch of *Fermi* in 2008, the combination of the Gamma-Ray Burst Monitor (GBM) [2] and the Large Area Telescope (LAT) [3] provides a remarkable energy range for GRB spectroscopy. It is better for studying the spectral properties and the prompt emission processes responsible for GRBs. The GBM alone covers a wider energy range than its predecessor telescopes. This allows us to extend the spectral analysis up to 40 MeV and is large enough to compute the L_{iso} in the energy ranges 1 keV–10 MeV and 1 keV–30 MeV. The correlation of the isotropic peak luminosity and the intrinsic peak energy has a potential to test cosmological models. In this work, we report the best-fit parameters of the L_{iso}–$E_{i,p}$ correlation at high redshift obtained from the maximum likelihood technique and the χ^2 minimization method.

2. Sample and method of data analysis

We select the brightest GRBs with known redshift concurrently detected by both *Fermi*-LAT and GBM in nine years of operations (up to the end of May 2017). In our sample, there are 25 long GRBs and one short GRB (observed duration $\lesssim 2$ s). GRBs with no break (peak) energy in the νF_ν energy spectrum and the bursts with statistics in the selected time interval too small to adequately constrain the parameters in the spectral fit are not included in our sample. The GBM comprises 12 Sodium Iodide (NaI) and 2 Bismuth Germanate (BGO) detectors that are sensitive in the 8 keV–1 MeV and 150 keV–40 MeV energy ranges, respectively [2]. For one-second peak flux duration, we have selected approximately 0.512 s before and after the reported T_{peak} for each burst. T_{peak} is a time when the lightcurve of GRB prompt emission peaks and this time is measured from the GRB trigger time T_0. The reason for using 0.512 s is that the *CSPEC* data we have used from *Fermi*-GBM has a time resolution of 1.024 s.

As in most of the previous spectral analysis of GRBs, we used the smoothly broken power law (SBPL) [4], power law function with an exponential high-energy cutoff [Comptonized (Comp)], Band function (Band) [5], Band plus extra thermal black-body (BB) component and SBPL + BB. For the detector selection, the criterion adopted by authors in reference [6] is implemented. To perform the spectral analysis, the *RMFIT* package [7] has been used. The NaI data from 10–915 keV and the BGO data from 210 keV–30 MeV are used by cutting out the overflowing low and high-energy channels as well as the K-edge from 30–40 keV. The background in each of the GBM detectors was estimated by fitting polynomial functions to the light curves in various energy ranges

before and after the source active time period. For GBM data, the background was fitted to the
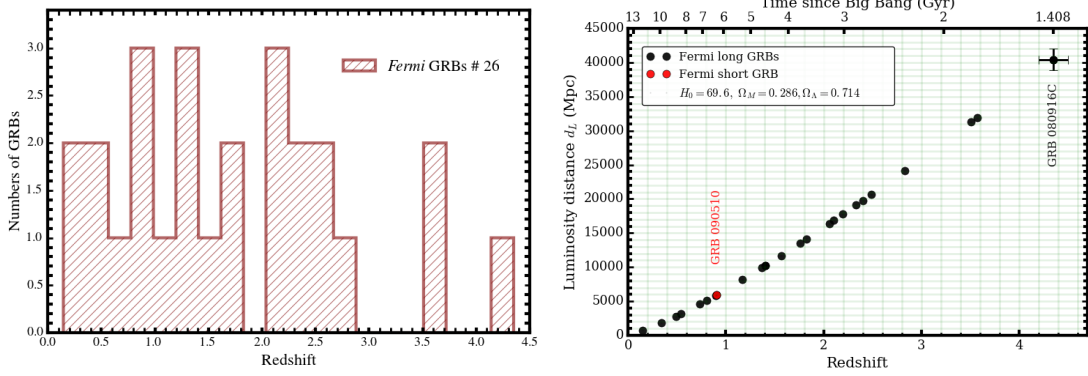

Figure 1: *Left side* – The histogram of the *Fermi* GRBs (25 long and one short GRBs). *Right side* – The luminosity distance d_L to GBM GRBs in ΛCDM cosmology with standard parameters of 25 long GRBs (black circles) and one short GRB (red circle). On the upper *x*-axis, the time since Big Bang (Gyr) shows the age of the Universe at different redshift *z*.

standard 128 energy bins of the *CSPEC* data-type which cover a much longer time range, making the estimation of the background more reliable for long GRBs [8]. Our sample is thus composed of 26 *Fermi* GBM GRBs with known redshift which is shown as histogram in the left side of Figure 1 and their luminosity distance d_L in ΛCDM cosmology with standard parameters (see the right side of Figure 1).

3. Spectral analysis

The spectral parameters of the best fit model for T_{peak} time-integrated spectral analysis are listed in Table 1. The spectra of GRBs in the keV–MeV energy range are usually constrained with the empirical Band function [5] (see the top left panel of Figure 2), although recent observations with *Fermi* revealed deviations from the Band model, in the form of an additional thermal BB component as shown in the bottom right panel of Figure 2. The SBPL model adequately fits the spectra of eight GRBs (top right panel) and the Comp model also fit the spectra of three GRBs as shown in the bottom left panel of Figure 2. The fit statistics used for the spectral analysis was the Castor statistic (C-stat), which is a variant of the log-likelihood introduced by Cash [9]. It is the modification of Cash-statistic [10] combined with the χ^2 statistic, thus it can be used to estimate a goodness of fit. In a few bursts (see the rows of Table 1 written in bold: GRB 170214A, GRB 130702A and GRB 131108) the high energy spectral index β larger than -2 is observed. This implies that the spectral peak energy or break energy was beyond the upper end of the fit range, νF_ν spectra, because the high energy data was not adequate to fix β. Hence we could not include those sources indicating no peak energy in the νF_ν spectra (Figure 2, shown by broken lines).

4. The analysis of L_{iso}–$E_{i,p}$ correlation

We derived the intrinsic peak energy, $E_{i,p}$ of the νF_ν spectrum in the cosmological rest frame, which typically shows a peak at a characteristic spectral peak energy (E_{peak}) or break energy (E_0).

Table 1: The result of the spectral fit parameters for a T$_{peak}$ time integrated spectral analysis of 26 GRBs.

GRB name	Detectors	Model	T$_{peak}$	α, γ	β	E$_p$, E$_0$	kT	C-Stat/dof[(*)]
GRB 170405A	n6+n7+n9+nb+b1	Band	29.504 - 30.528	-0.57 ±0.06	-2.22 ± 0.16	314.8 ± 28.1		651.05/581
GRB 170214A	**n0+n1+n3+b0**	**Band**	**61.696 - 62.784**	**-0.67 ± 0.06**	**-1.91 ± 0.07**	**489.0 ± 56.3**		**495.84/465**
GRB 160625B	n7+n9+b1	SBPL+BB	188.672 - 189.760	-0.74 ± 0.02	-2.33 ± 0.03	565.2 ± 27.2	39.42 ± 1.26	635.87/344
GRB 160509A	n0+n1+n3+b0	SBPL	16.576 - 17.664	-0.87 ± 0.02	-2.16 ± 0.04	203.1 ± 11.2		542.14/465
GRB 150514A	n3+n6+n7+b0	SBPL	0.448 - 1.024	-1.07 ± 0.11	-2.81 ± 0.29	91.43 ± 20.5		504.34/465
GRB 150403A	n3+n4+b0	Band	11.072 - 12.160	-0.70± 0.03	-2.18 ± 0.08	580.4 ± 38.1		415.50/348
GRB 150314A	n0+n1+n9+na+B0+b1	Band	2.112 - 3.200	-0.40 ± 0.02	-2.58 ± 0.07	300.7 ± 7.0		956.79/701
GRB 141028A	n6+n7+n9+b1	Band	12.608 - 13.632	-0.61 ± 0.06	-2.18 ± 0.13	352.1 ± 31.5		459.06/464
GRB 131108A	**n0+n3+n7+b0**	**SBPL**	**1.152-0.064**	**-0.69 ± 0.05**	**-1.99 ± 0.05**	**153.20 ± 14.50**		**762.48/706**
GRB 130702A	**n6+n7+n8+b1**	**Band**	**1.472 - 2.560**	**-0.69 ± 0.73**	**-1.98 ± 0.13**	**53.07 ± 24.0**		**482.13/465**
GRB 130518A	n3+n6+n7+b0+b1	Band	25.600 - 26.624	-0.75 ± 0.02	-2.31 ± 0.07	523.0 ± 24.3		655.55/589
GRB 130427A	n6+n9+na+b1	Band+BB	11.072 - 12.096	-0.67 ± 0.03	-2.38 ± 0.03	305.7 ± 9.32	15.93 ± 0.87	474.92/345
GRB 120711A	n2+na+b0+b1	SBPL	94.464 - 95.552	-0.85 ± 0.03	-2.30 ± 0.08	693.0 ± 73.5		505.73/469
GRB 120624B	n1+n2+na+b0+b1	SBPL	11.392 - 12.416	-0.88 ± 0.04	-2.20 ± 0.13	311.6 ± 46.9		640.73/588
GRB 110731A	n0+n1+n6+n7+n9+b0+b1	Comp	-0.320 - 0.768	-0.98 ± 0.07		168.0 ± 12.0		882.21/820
GRB 100728A	n0+n1+n2+n5+b0	SBPL	80.192 - 81.280	-0.58 ± 0.07	-2.35 ± 0.25	272.9 ± 51.4		672.34/583
GRB 100414A	n7+n9+n11+b1	Band	22.784 - 23.872	-0.68 ± 0.05	-2.87 ± 0.53	544.9 ± 43.6		479.97/465
GRB 091127	n6+n7+n9+b1	Band	0.960 - 2.048	-1.31 ± 0.04	-2.19 ± 0.07	135.8 ± 13.0		533.09/463
GRB 091003A	n0+n3+n6+b0+b1	Band	18.048 - 19.136	-0.66 ± 0.03	-2.90 ± 0.28	432.8 ± 19.6		647.32/586
GRB 090926A	n6+n7+n8+b1	Band	3.776 - 4.864	-0.45 ± 0.03	-2.24 ± 0.04	264.8 ± 7.69		580.86/468
GRB 090902B	n0+n2+n9+b0+b1	SBPL	13.952 - 15.040	-0.86 ± 0.01	-3.41 ± 0.21	672.4 ± 45.2		753.77/586
GRB 090510	n3+n6+n7+n9+b0+b1	SBPL	0.00 - 1.088	-0.87 ± 0.02	-2.80 ± 0.24	3109.0 ± 480.0		687.16/698
GRB 090424	n7+n8+nb+b1	Band	0.768 - 1.856	-0.83 ± 0.02	-3.40 ± 0.29	202.7 ±,4.75		573.63/465
GRB 090328	n7+n8+b1	Comp	23.488 - 24.512	-0.73 ± 0.05		489.0,± 40.9		448.39/352
GRB 090323	n6+n7+n9+n11+b1	Comp	66.176 - 67.264	-0.54 ± 0.07		381.2 ± 33.2		595.80/579
GRB 080916C	n3+n4+b0	Band	0.832 - 1.920	-0.31 ± 0.13	-2.07 ± 0.17	402.2 ± 63.9		391.46/353

Notes. α and β are the lower and higher photon indices for Band and SBPL functions, respectively. E_0 is the SBPL e-folding energy in keV. γ is a photon spectral index of Comp model. E_p is the Band and Comp spectral peak energy in keV and kT is the parameter of black body temperature in keV. dof[(*)] is the degrees of freedom associated to the spectra of the GRBs.

We also computed the intrinsic peak luminosity in the cosmological source frame,

$$L_{iso} = 4\pi d_L^2 P_{bolo}, \tag{4.1}$$

where $P_{bolo} = \int_{E_{min}/(1+z)}^{E_{max}/(1+z)} E N_i(E) dE$ erg cm^{-2} s^{-1} is the bolometric peak flux integrated over the minimum energy E_{min} = 1 keV and the maximum energy $E_{max} = 10^4$ keV or 3×10^4 keV. Here, $N_i(E)$ represents the best-fit spectral models. Assuming a flat ΛCDM model with the density of dark matter $\Omega_m = 1 - \Omega_\Lambda$, the d_L can be expressed with Hubble expansion rate

$$d_L = (1+z)\frac{c}{H_0} \int_0^z \frac{dz'}{\sqrt{(1-\Omega_\Lambda)(1+z')^3 + \Omega_\Lambda}}, \tag{4.2}$$

where Ω_Λ is the dark energy density at present, and H_0 (km s^{-1} Mpc^{-1}) is the Hubble constant. The result of d_L, L_{iso}, $E_{i,p}$ and P_{bolo} are reported in Table 2. The Yonetoku relation L_{iso}–$E_{i,p}$ can be parametrized as follows:

$$\log \frac{L_{iso}}{\text{erg s}^{-1}} = k + m \log \frac{E_{i,p}}{\text{keV}}, \tag{4.3}$$

where k and m are the intercept and slope, respectively. To standardize the equation (4.3), we need to fit the correlated data $\{x_i, y_i\}$ with uncertainties $\{\sigma_{xi}, \sigma_{yj}\}$, to the linear relation $y = k + mx$. Thus, the expression of the L_{iso}–$E_{i,p}$ plane should be written as $y = \log \frac{L_{iso}}{\text{erg s}^{-1}}$ and $x = \log \frac{E_{i,p}}{\text{keV}}$. The parameter of y should not only depend on x, but also depend on a certain amount of an extrinsic
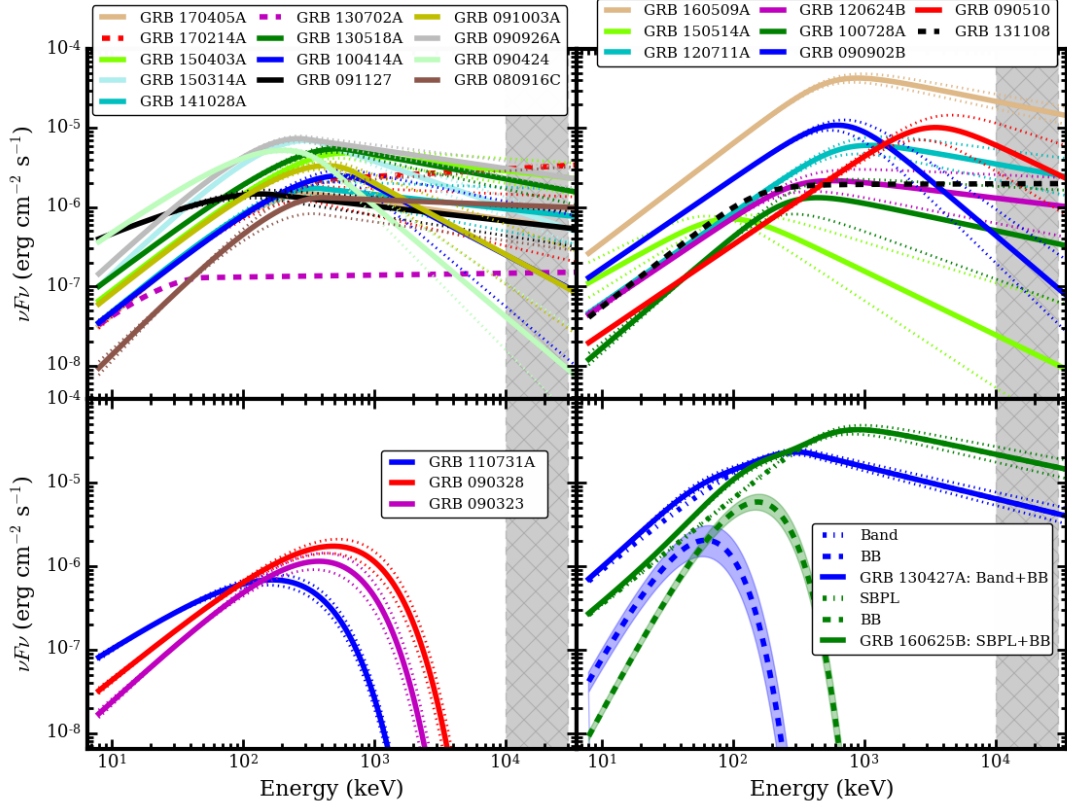
Figure 2: The νF_ν spectra of *Fermi*-GBM GRBs with known redshift resulting from one second time integrated spectral analysis. *Top left panel* – Shows the best fit Band models. *Top right panel* – Shows the best fit SBPL models. *Bottom left panel* – Indicates the best fit Comp models. *Bottom right panel* – Shows the best fit spectra fit by models with a BB component. The solid and dotted lines correspond to the best-fit models and the 1σ confidence region of the models, respectively. For GRB 170214A (dashed red), GRB 130702A (dashed magenta) and GRB 131108 (dashed black), we could not find the peak of νF_ν spectra.

variance (σ_{ext}) parameter that accounts for hidden parameters related to GRB intrinsic physical mechanisms. The parameters k, m and σ_{ext} are obtained through the χ^2 minimization given by

$$\chi^2 = \sum_{i=1}^{N} \frac{(y_i - k - m x_i)^2}{\sigma_{y_i}^2 + m^2 \sigma_{x_i}^2 + \sigma_{ext}^2}, \qquad (4.4)$$

where N is the number of GRBs. We also apply the likelihood function [11] which accounts for uncertainties on both the x and y quantities:

$$\mathscr{L}(k, m, \sigma_{ext}) = \frac{1}{2} \sum_{i=0}^{N} \ln(\sigma_{ext}^2 + \sigma_{y_i}^2 + m^2 \sigma_{x_i}^2) + \frac{1}{2} \sum_{i=0}^{N} \frac{(y_i - m x_i - k)^2}{\sigma_{ext}^2 + \sigma_{y_i}^2 + m^2 \sigma_{x_i}^2}. \qquad (4.5)$$

By maximizing the likelihood expressed in equation (4.5), we can constrain the extrinsic scatter parameter σ_{ext}, and the coefficients of the L_{iso}–$E_{i,p}$ correlation, simultaneously.

Table 2: $E_{\rm i,p}$, $L_{\rm iso}$ and $P_{\rm bolo}$ in the GRB rest frame with the luminosity distance and redshift.

GRB	z	$d_{\rm L}$ (cm)	$E_{\rm i,p}$ (keV)	$P_{\rm bolo}^{10}$ (erg cm^{-2} s^{-1})	$L_{\rm iso}^{10}$ (erg s^{-1})	$P_{\rm bolo}^{30}$ (erg cm^{-2} s^{-1})	$L_{\rm iso}^{30}$ (erg s^{-1})
GRB 170405A	3.51[a]	9.66×10^{28}	1420.42 ± 127.86	$(0.45 \pm 0.02) \times 10^{-5}$	$(5.29 \pm 0.25) \times 10^{53}$	$(0.55 \pm 0.05) \times 10^{-5}$	$(6.42 \pm 0.60) \times 10^{53}$
GRB 170214A	2.53[b]	6.51×10^{28}	-	$(0.82 \pm 0.03) \times 10^{-5}$	$(4.37 \pm 0.14) \times 10^{53}$	$(1.16 \pm 0.06) \times 10^{-5}$	$(6.15 \pm 0.34) \times 10^{53}$
GRB 160625B	1.406[c]	3.16×10^{28}	2157.05 ± 59.11	$(12.53 \pm 0.15) \times 10^{-5}$	$(1.57 \pm 0.02) \times 10^{54}$	$(15.46 \pm 0.23) \times 10^{-5}$	$(1.94 \pm 0.03) \times 10^{54}$
GRB 160509A	1.17[d]	2.51×10^{28}	864.68 ± 59.87	$(2.59 \pm 0.11) \times 10^{-5}$	$(2.06 \pm 0.09) \times 10^{53}$	$(3.10 \pm 0.18) \times 10^{-5}$	$(2.46 \pm 0.14) \times 10^{53}$
GRB 150514A	0.807[e]	1.59×10^{28}	175.68 ± 15.79	$(0.13 \pm 0.01) \times 10^{-5}$	$(4.06 \pm 0.35) \times 10^{51}$	$(0.13 \pm 0.01) \times 10^{-5}$	$(4.11 \pm 0.40) \times 10^{51}$
GRB 150403A	2.06[f]	5.06×10^{28}	1775.61 ± 115.21	$(1.54 \pm 0.04) \times 10^{-5}$	$(4.95 \pm 0.12) \times 10^{53}$	$(1.92 \pm 0.08) \times 10^{-5}$	$(6.18 \pm 0.26) \times 10^{53}$
GRB 150314A	1.758[g]	4.16×10^{28}	829.82 ± 19.26	$(2.05 \pm 0.04) \times 10^{-5}$	$(4.48 \pm 0.08) \times 10^{53}$	$(2.21 \pm 0.06) \times 10^{-5}$	$(4.82 \pm 0.14) \times 10^{53}$
GRB 141028A	2.33[h]	5.89×10^{28}	1171.93 ± 105.39	$(0.56 \pm 0.03) \times 10^{-5}$	$(2.45 \pm 0.11) \times 10^{53}$	$(0.68 \pm 0.06) \times 10^{-5}$	$(2.97 \pm 0.25) \times 10^{53}$
GRB 131108A	2.40[i]	6.10×10^{28}	-	$(0.74 \pm 0.04) \times 10^{-5}$	$(3.48 \pm 0.14) \times 10^{53}$	$(0.98 \pm 0.04) \times 10^{-5}$	$(4.58 \pm 0.20) \times 10^{53}$
GRB 130702A	0.145[j]	0.21×10^{28}	-	$(0.04 \pm 0.20) \times 10^{-5}$	$(2.18 \pm 10.1) \times 10^{49}$	$(0.05 \pm 0.21) \times 10^{-5}$	$(2.58 \pm 11.8) \times 10^{49}$
GRB 130518A	2.49[k]	6.38×10^{28}	1824.19 ± 84.90	$(1.60 \pm 0.03) \times 10^{-5}$	$(8.17 \pm 0.14) \times 10^{53}$	$(1.92 \pm 0.06) \times 10^{-5}$	$(9.80 \pm 0.29) \times 10^{53}$
GRB 130427A	0.3399[l]	0.56×10^{28}	409.50 ± 12.50	$(8.23 \pm 0.10) \times 10^{-5}$	$(3.23 \pm 0.04) \times 10^{52}$	$(8.89 \pm 0.15) \times 10^{-5}$	$(3.49 \pm 0.06) \times 10^{52}$
GRB 120711A	1.405[m]	3.15×10^{28}	2674.59 ± 170.42	$(1.74 \pm 0.05) \times 10^{-5}$	$(2.18 \pm 0.06) \times 10^{53}$	$(2.21 \pm 0.08) \times 10^{-5}$	$(2.76 \pm 0.10) \times 10^{53}$
GRB 120624B	2.1974[n]	5.48×10^{28}	1811.75 ± 240.83	$(0.68 \pm 0.03) \times 10^{-5}$	$(2.58 \pm 0.10) \times 10^{53}$	$(0.85 \pm 0.06) \times 10^{-5}$	$(3.20 \pm 0.22) \times 10^{53}$
GRB 110731A	2.83[o]	7.45×10^{28}	643.41 ± 45.48	$(0.20 \pm 0.01) \times 10^{-5}$	$(1.39 \pm 0.05) \times 10^{53}$	$(0.20 \pm 0.01) \times 10^{-5}$	$(1.39 \pm 0.06) \times 10^{53}$
GRB 100728A	1.567[p]	3.61×10^{28}	1144.75 ± 148.41	$(0.43 \pm 0.04) \times 10^{-5}$	$(6.97 \pm 0.66) \times 10^{52}$	$(0.49 \pm 0.08) \times 10^{-5}$	$(8.11 \pm 1.31) \times 10^{52}$
GRB 100414A	1.368[q]	3.05×10^{28}	1291.62 ± 104.26	$(0.71 \pm 0.06) \times 10^{-5}$	$(8.32 \pm 0.67) \times 10^{52}$	$(0.75 \pm 0.11) \times 10^{-5}$	$(8.77 \pm 1.29) \times 10^{52}$
GRB 091127	0.49[r]	0.86×10^{28}	201.94 ± 19.49	$(0.79 \pm 0.04) \times 10^{-5}$	$(7.42 \pm 0.34) \times 10^{51}$	$(0.87 \pm 0.06) \times 10^{-5}$	$(8.13 \pm 0.53) \times 10^{51}$
GRB 091003A	0.8969[s]	1.81×10^{28}	819.27 ± 38.04	$(0.97 \pm 0.04) \times 10^{-5}$	$(3.97 \pm 0.18) \times 10^{52}$	$(1.00 \pm 0.07) \times 10^{-5}$	$(4.11 \pm 0.27) \times 10^{52}$
GRB 090926A	2.1062[t]	5.20×10^{28}	822.82 ± 23.92	$(2.54 \pm 0.04) \times 10^{-5}$	$(8.64 \pm 0.14) \times 10^{53}$	$(2.97 \pm 0.05) \times 10^{-5}$	$(1.00 \pm 0.03) \times 10^{54}$
GRB 090902B	1.822[u]	4.35×10^{28}	1767.04 ± 46.04	$(2.69 \pm 0.05) \times 10^{-5}$	$(6.41 \pm 0.12) \times 10^{53}$	$(2.81 \pm 0.08) \times 10^{-5}$	$(6.69 \pm 0.19) \times 10^{53}$
GRB 090510	0.903[v]	1.82×10^{28}	6731.81 ± 475.04	$(1.90 \pm 0.08) \times 10^{-5}$	$(7.94 \pm 0.31) \times 10^{52}$	$(2.71 \pm 0.11) \times 10^{-5}$	$(1.13 \pm 0.05) \times 10^{53}$
GRB 090424	0.544[w]	0.98×10^{28}	312.90 ± 7.29	$(1.52 \pm 0.04) \times 10^{-5}$	$(1.82 \pm 0.05) \times 10^{52}$	$(1.52 \pm 0.04) \times 10^{-5}$	$(1.83 \pm 0.05) \times 10^{52}$
GRB 090328	0.736[x]	1.42×10^{28}	849.54 ± 70.58	$(0.42 \pm 0.02) \times 10^{-5}$	$(1.06 \pm 0.56) \times 10^{53}$	$(0.42 \pm 0.02) \times 10^{-5}$	$(1.06 \pm 0.57) \times 10^{52}$
GRB 090323	3.57[y]	9.86×10^{28}	1743.24 ± 153.41	$(0.27 \pm 0.02) \times 10^{-5}$	$(3.32 \pm 0.21) \times 10^{53}$	$(0.27 \pm 0.02) \times 10^{-5}$	$(3.33 \pm 0.21) \times 10^{53}$
GRB 080916C	4.35 ± 0.15[z]	$(12.48 \pm 0.5) \times 10^{28}$	1938.69 ± 326.87	$(0.41 \pm 0.03) \times 10^{-5}$	$(8.01 \pm 0.81) \times 10^{53}$	$(0.62 \pm 0.06) \times 10^{-5}$	$(1.20 \pm 0.14) \times 10^{54}$

Notes. $L_{\rm iso}^{10}$ and $L_{\rm iso}^{30}$ are the isotropic luminosity computed in the $1\text{–}10^4$ keV and $1\text{–}3 \times 10^4$ keV energy ranges, respectively. $P_{\rm bolo}^{10}$ and $P_{\rm bolo}^{30}$ are the bolometric flux over a one second interval computed in the $1\text{–}10^4$ keV and $1\text{–}30^4$ keV energy ranges, respectively. Here, we use a standard ΛCDM parameters $H_0 = 69.6$ km s^{-1} Mpc^{-1}, $\Omega_{\rm m} = 0.286$ and $\Omega_\Lambda = 0.714$, respectively. The GRBs for which there is no value for $E_{\rm i,p}$ are not included.

References for the redshift: (*a*) de Ugarte Postigo et al. GCN 20990 (2017), (*b*) Kruehler et al. GCN 20686 (2017); Kruehler et al. GCN (2017), (*c*) Tanvir et al. GCN 19600 (2016), (*d*) Tanvir et al. GCN 19419 (2016), (*e*) de Ugarte Postigo et al. GCN 17822 (2015), (*f*) Pugliese et al. GCN 17672 (2015), (*g*) de Ugarte Postigo et al. GCN 17583 (2015), (*h*) Xu et al. GCN 16983 (2014), *i*) de Ugarte Postigo et al. GCN 15470 (2013), *j*) Leloudas et al. GCN 14983 (2013), (*k*) Sánchez-Ramírez et al. GCN 14685 (2013); Cucchiara et al. GCN 14687 (2013), (*l*) Xu et al. (2013), APJ, 776, (*m*) Tanvir et al. GCN 13441 (2012), (*n*) de Ugarte Postigo et al. (2013), AAP, 557, (*o*) Tanvir et al. GCN 12225 (2011), (*p*) Kruehler et al. GCN 14500 (2010), (*q*) Cucchiara and Fox GCN 10606 (2010), (*r*) Cucchiara et al. GCN 10202 (2009), (*s*) Cucchiara et al. GCN 10031 (2009), (*t*) Malesani et al. GCN 9942 (2009), (*u*) Cucchiara et al. GCN 9873 (2009), (*v*) Rau et al. GCN 9353 (2009), (*w*) Chornock et al. GCN 9243 (2009), (*x*) Cenko et al. GCN 9053 (2009), (*y*) Chornock et al. GCN 9028 (2009), (*z*) Greiner et al. (2009), A&A, 498; Atwood et al. (2013), APJ, 774.

In Figure 3 we show the $L_{\rm iso}$–$E_{\rm i,p}$ correlation for 22 long *Fermi* GBM GRBs (short GRB 090510 is not included). As in the previous computations [1], $L_{\rm iso}$ is derived in the 1 keV–10 MeV energy range (F10). Since the GBM observes GRBs up to 40 MeV, we extended the computation of $L_{\rm iso}$ to 30 MeV (F30). The $L_{\rm iso}$, $E_{\rm i,p}$ and $P_{\rm bolo}$ of the GRBs with redshift are reported in Table 2. To compute the $P_{\rm bolo}$ and its uncertainty, we have performed the Monte Carlo simulations by assuming the spectral fitting parameters are correlated and follow a multivariate Gaussian function. We generate 10000 sets of random values for each of the best-fit spectral model parameters using the covariance matrix generated by *RMFIT*. Next, we calculate $P_{\rm bolo}$ for the 10000 sets of random values mentioned above. The most probable value (MPV) of $P_{\rm bolo}$ is then found from the peak of the distribution of 10000 random values. The error on $P_{\rm bolo}$ is computed from the 68 % confidence level in the symmetric interval, centred on the MPV. Then using these values, we computed the $L_{\rm iso}$ (Eq 4.1) and its uncertainty.

5. Discussion

The result presented in this work is constructed based on the distribution of energetic *Fermi* GBM GRBs with measured redshift and homogeneous energy range selection criteria during the spectral analysis. The spectra of these GRBs integrated over T_{peak} are constrained by different models, such as Band, Comp, SBPL, Band + BB and SBPL + BB functions. We found that the L_{iso}– $E_{\mathrm{i,p}}$ correlation for the *Fermi* long GRBs is rather strong and only the short GRB 090510 appears as an outlier. For F10, considering our correlation in equation (4.5) the likelihood analysis method gives $m = 1.81 \pm 0.24$, $k = 51.37 \pm 0.29$ and $\sigma_{\mathrm{ext}} = 0.43 \pm 0.06$. The value of σ_{ext} is 0.447 when the reduced χ^2 is unity but the constrained parameters are quite similar to the likelihood method. The Spearman's correlation coefficient indicates a positive high correlation of 0.815. For the correlation of L_{iso} computed over 1 keV–30 MeV energy range (F30) with $E_{\mathrm{i,p}}$, we also found a very significant Spearman's correlation coefficient, $\rho_{\mathrm{sp}} = 0.82$. Using a likelihood function we obtain $m = 1.88 \pm 0.17$, $k = 51.35 \pm 0.24$ and $\sigma_{\mathrm{ext}} = 0.42 \pm 0.04$. The reduced χ^2 is unity when the σ_{ext} is 0.457. By computing L_{iso} from 1 keV to 30 MeV, the slope of the correlation becomes slightly steeper than the L_{iso} computed over 1 keV–10 MeV energy range, while its extrinsic variance does not change significantly.
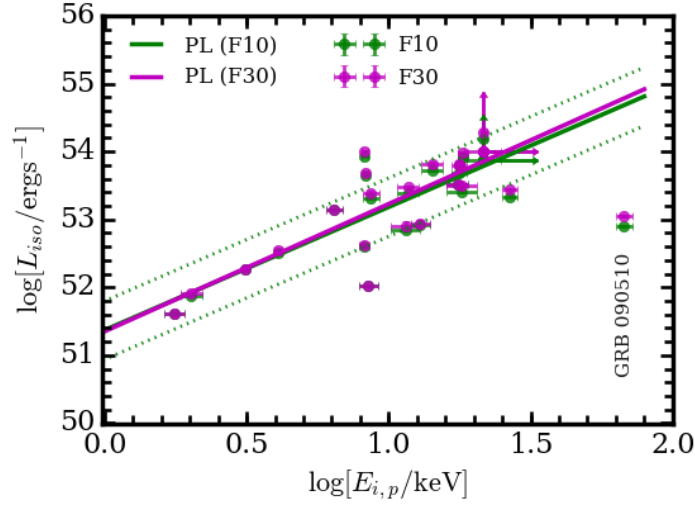

Figure 3: The best fits are shown by solid lines which are obtained from the maximum likelihood method for constant ΛCDM. F10 (green) and F30 (magenta) representing the L_{iso} computed over the energy range (1 keV–30 MeV) and (1 keV–30 MeV), respectively. The dotted green line shows the $1\sigma_{\mathrm{ext}}$ extrinsic scatter around the best fit of the F10 sample obtained by minimizing the likelihood function.

Our results show that the L_{iso}–$E_{\mathrm{i,p}}$ correlation is a promising tool to probe the high-redshift Universe. Interestingly, the *Fermi* GBM GRBs detected up to 30 MeV lie perfectly along the previous fit of Yonetoku relation [12]. These very bright GRBs are concentrated in the upper right of the L_{iso}–$E_{\mathrm{i,p}}$ plane and increase the significance of the correlation.

Acknowledgments

References

[1] Yonetoku D, Murakami T, Nakamura T, Yamazaki R, Inoue A and Ioka K 2004 *The Astrophysical Journal* **609** 935

[2] Meegan C, Lichti G, Bhat P, Bissaldi E, Briggs M S, Connaughton V, Diehl R, Fishman G, Greiner J, Hoover A S *et al.* 2009 *The Astrophysical Journal* **702** 791

[3] Atwood W, Abdo A A, Ackermann M, Althouse W, Anderson B, Axelsson M, Baldini L, Ballet J, Band D, Barbiellini G *et al.* 2009 *The Astrophysical Journal* **697** 1071

[4] Ryde F 1999 *Astrophysical Letters and Communications* **39** 281

[5] Band D, Matteson J, Ford L, Schaefer B, Palmer D, Teegarden B, Cline T, Briggs M, Paciesas W, Pendleton G *et al.* 1993 *The Astrophysical Journal* **413** 281–292

[6] Guiriec S, Connaughton V, Briggs M S, Burgess M, Ryde F, Daigne F, Mészáros P, Goldstein A, McEnery J, Omodei N *et al.* 2011 *The Astrophysical Journal Letters* **727** L33

[7] *https://fermi.gsfc.nasa.gov/ssc/data/analysis/rmfit/*

[8] Guiriec S, Kouveliotou C, Daigne F, Zhang B, Hascoët R, Nemmen R, Thompson D, Bhat P, Gehrels N, Gonzalez M *et al.* 2015 *The Astrophysical Journal* **807** 148

[9] Cash W 1979 *The Astrophysical Journal* **228** 939–947

[10] *https://heasarc.nasa.gov/docs/xanadu/xspec/xspec11/manual/node57.html*

[11] D'Agostini G 2005 *ArXiv Physics e-prints*

[12] Ghirlanda G, Nava L, Ghisellini G, Celotti A, Burlon D, Covino S and Melandri A 2012 *Monthly Notices of the Royal Astronomical Society* **420** 483–494